



Fermi National Accelerator Laboratory

FERMILAB-FN-630

**Potential-Well Distortion and Mode-Mixing
Instability in Proton Machines**

K. Ng

*Fermi National Accelerator Laboratory
P.O. Box 500, Batavia, Illinois 60510*

August 1995

Disclaimer

This report was prepared as an account of work sponsored by an agency of the United States Government. Neither the United States Government nor any agency thereof, nor any of their employees, makes any warranty, expressed or implied, or assumes any legal liability or responsibility for the accuracy, completeness, or usefulness of any information, apparatus, product, or process disclosed, or represents that its use would not infringe privately owned rights. Reference herein to any specific commercial product, process, or service by trade name, trademark, manufacturer, or otherwise, does not necessarily constitute or imply its endorsement, recommendation, or favoring by the United States Government or any agency thereof. The views and opinions of authors expressed herein do not necessarily state or reflect those of the United States Government or any agency thereof.

POTENTIAL-WELL DISTORTION AND MODE-MIXING INSTABILITY IN PROTON MACHINES

King-Yuen Ng

Fermi National Accelerator Laboratory, P.O. Box 500, Batavia, IL 60510*

Abstract

In proton machines, potential-well distortion leads to small amount of bunch lengthening with minimal head-tail asymmetry. Longitudinal mode-mixing instability occurs at higher azimuthal modes. When the driving resonance is of broad-band, the threshold corresponds to the Boussard-modified Keil-Schnell criterion for microwave instability. [1] When the driving resonance is narrower than the bunch spectrum, the threshold corresponds to a similar criterion derived before. [2] The thresholds are higher when the machine operates below transition.

I. INTRODUCTION

Proton bunches are very much different from electron bunches. First, electron bunches have a length roughly equal to or shorter than the radius of the beam pipe, whereas proton bunches are usually very much longer. Second, the momentum spread of the electron bunches is determined by the heavy synchrotron radiation. Protons do not radiate and behave quite differently in the longitudinal phase space, with the bunch area conserved instead. These differences lead to different results in potential-well distortion and mode mixing. [3]

II. DISTORTION ASYMMETRY

As an example, the bunches in the Fermilab Main Ring have a typical full length of ~ 60 cm or $\tau_L \sim 2$ ns. The spectrum has a half width of $\sim \tau_L^{-1} = 0.5$ GHz. Therefore, the static bunch profile is hardly affected by the resistive part of the broad-band impedance which is centered at $1.5 \sim 4$ GHz. As a result, the inductive part of the broad-band will only lead to a symmetric broadening (shortening) of the bunch above (below) transition. This conjecture can be tested by means of the Haïssinski equation [4]. Strictly speaking, the Haïssinski equation does not apply to proton bunches where the bunch area is conserved and the momentum spread is not a fixed Gaussian. Nevertheless, it should give us an idea of the amount of asymmetric head-tail distortion. Adapting the Main Ring bunch at $E = 150$ GeV to a longitudinal Gaussian profile, we take the bunch area as $A = 6\pi\sigma_\tau\sigma_E = 0.15$ eV-sec, where σ_τ and σ_E are the rms bunch length in time and rms energy spread. With a

*Operated by the Universities Research Association, Inc., under contract with the U.S. Department of Energy.

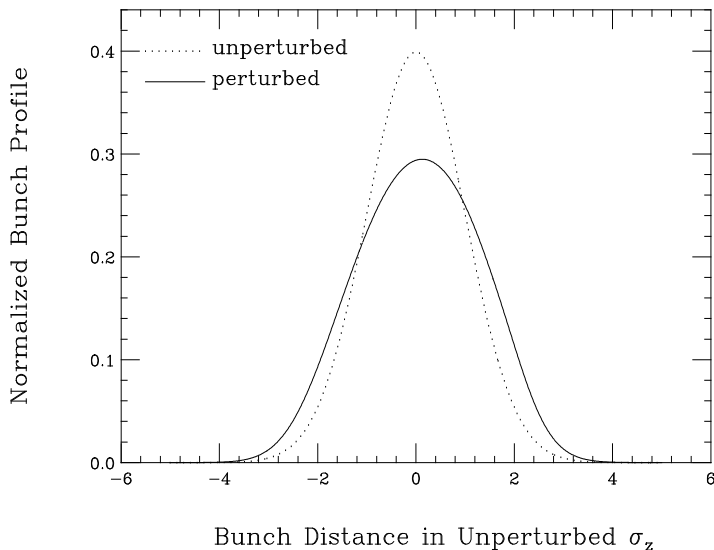


Fig. 1. An estimate of potential-well distortion of a Main Ring bunch from the solution of Haüssinski equation. Note that the head-tail asymmetry is very small.

revolution frequency of $f_0 = \omega_0/2\pi = 47.7$ kHz, a phase-slip parameter of $\eta = 0.0028$, and an unperturbed synchrotron tune of $\nu_{s0} = \omega_{s0}/\omega_0 = 0.00361$, we obtain an unperturbed rms bunch length of $\sigma_\tau = \sqrt{\frac{\eta A}{6\pi\omega_{s0}E\beta^2}} = 0.37$ ns or 11 cm. This profile is plotted as dashes in Fig. 1. At present, the Main Ring bunch has an intensity of $N = 4.5 \times 10^{10}$ protons and the Main Injector under construction has a designed intensity of $N = 6.0 \times 10^{10}$. The broad-band impedance of the Main Ring is believed to be $Z/n \approx 5$ to 10Ω and the cut-off frequency is ~ 4 GHz, while the broad-band impedance of the Main Injector is $Z/n \lesssim 1 \Omega$. Here, we take as illustration $N(Z/n) = 60 \times 10^{10} \Omega$ with the broad-band impedance centered at 2 GHz. The self-consistent Haüssinski equation is then solved and the impedance-distorted bunch profile is plotted as solid in Fig. 1. We can see that the asymmetry in the distortion is indeed extremely small.

III. POTENTIAL-WELL LENGTHENING

When the small asymmetry in the potential-well distortion is neglected, we can considered the driving impedance to be pure inductive. The wake potential is the derivative of the δ -function. For a parabolic bunch, the wake force will be linear and can be superimposed onto the linearized rf force easily. The potential-well distorted bunch will therefore remain parabolic. For this reason, the distribution in longitudinal phase space should be, [5]

$$\psi(\tau, \delta) = \frac{3\eta cN}{2\pi\omega_{s0}\hat{\tau}_0^3} \sqrt{\hat{\tau}_0^2 - \frac{1}{\kappa} \left(\frac{\eta}{\omega_{s0}} \delta \right)^2 - \kappa\tau^2}, \quad (3.1)$$

where we have used as conjugate variables: τ , the time of arrival with respect to the synchronous particle, and $-\eta\delta/\omega_{s0}$ where δ is the momentum spread. The independent “time”

variable is s , the distance along the ring. The original half length of the bunch $\hat{\tau}_0$ has been lengthened to $\hat{\tau}_0/\sqrt{\kappa}$, whereas the momentum spread δ is shortened by $\sqrt{\kappa}$, so that the bunch area remains the same. Throughout this paper, the particles are considered to be ultra-relativistic, so that their longitudinal velocities are taken to be c , the velocity of light. With the addition of the inductive wake potential, the Hamiltonian is modified to

$$H = \frac{\eta^2}{2\omega_{s0}c} \delta^2 + \frac{\omega_{s0}}{2c} (1 - D\kappa^{3/2}) \tau^2, \quad (3.2)$$

where

$$D = \frac{3e^2 N \eta}{4\pi \omega_{s0}^2 E \hat{\tau}_0^3} \frac{Z}{n} \Big|_{\text{ind}}. \quad (3.3)$$

The incoherent synchrotron angular frequency is therefore $\omega_s = \omega_{s0}(1 - D\kappa^{3/2})^{1/2}$. Since the distribution $\psi(\tau, \delta)$ must be a function of the Hamiltonian, to conform with Eq. (3.1), we have

$$\psi(\tau, \delta) = \frac{3\eta c N}{2\pi \omega_{s0} \hat{\tau}_0^3} \sqrt{\hat{\tau}_0^2 - \frac{2c}{\kappa \omega_{s0}} H}, \quad (3.4)$$

with the constraint

$$\kappa^2 = 1 - D\kappa^{3/2}. \quad (3.5)$$

Again, consider a 150 GeV Main Ring bunch with $N = 4.5 \times 10^{10}$ of bunch area 0.15 eV-sec and an inductive impedance of $Z/n|_{\text{ind}} \approx 20 \times 10^{10}$ Ohms. Then $D = 0.204$, indicating that the bunch has been lengthened by $\kappa^{-1/2} = 1.05$ and the momentum spread flattened by 5%. This implies that we cannot infer the momentum spread naively through the relation $\hat{\delta} = \omega_{s0} \tau_L / \eta$ by measuring the bunch length and the synchrotron frequency, because the answer will be $\sim 10\%$ too large, giving a wrong idea about the amount of Landau damping. Instead, the momentum spread should be measured from Schottky signals or inferred through dispersion from the measurement of the transverse profile of the bunch using a flying wire.

IV. MODE-MIXING

The coherent bunch modes will be shifted by the impedance of the vacuum chamber. As the current increases, two modes will collide to give an instability. It was illustrated in Sec. II that the potential-well distortion has very little head-tail asymmetry, indicating that radial modes will not be important and will be neglected. However, we do want to keep the effect of the potential-well modification; therefore, the perturbed ω_s will be used in below. In fact, going from the coordinates (τ, δ) to the polar coordinates (r, ϕ) , where

$$\begin{cases} \tau = r \cos \phi, \\ -\frac{\eta}{\omega_s} \delta = r \sin \phi, \end{cases} \quad (4.1)$$

the potential-well lengthening of the bunch discussed in Sec. III has been included already.

The shifts of the synchrotron side-bands can be derived using Vlasov equation. Here, we follow the Sacherer's approach. [6] The bunch profile of the i -th coherent mode can be written as

$$\rho^{(i)}(\tau) = \sum_k \alpha_k^{(i)} \lambda_k(\tau) , \quad (4.2)$$

where $\lambda_k(\tau)$ denotes a set of normalized orthogonal profile functions with k nodes between $-\frac{1}{2}\tau_L$ and $+\frac{1}{2}\tau_L$, with τ_L denoting the total length of the bunch. It can be shown that (see Appendix) $\alpha_m^{(i)}$ satisfies the equations

$$\sum_k [(\Omega^{(i)} - m\omega_s)\delta_{mk} - M_{mk}] \alpha_k^{(i)} , \quad (4.3)$$

for all m 's. In other words, $(\alpha_1^{(i)}, \alpha_2^{(i)}, \dots)$ is the i -th eigenvector corresponding to the eigenvalue $\Omega = \Omega^{(i)}$. In the above, the coupling matrix is given by

$$M_{mk} = -\frac{i\omega_s\omega_0 I_b}{3B_0^3 h V_T \cos \varphi_s} \frac{m}{m+1} \frac{\sum_n h_{mk}(\omega') Z(\omega')/\omega'}{\sum_n h_{mm}(\omega')} \quad (4.4)$$

where $\omega' = n\omega_0 + \Omega$, V_T is the potential-well modified rf voltage, which is related to the unperturbed rf voltage V_0 by $V_T/V_0 = (\omega_s/\omega_{s0})^2$, φ_s is the synchronous phase, h is the rf harmonic, I_b is the average bunch current, $B_0 = \tau_L f_0$ is the bunching factor, and $h_{mk}(\omega') = \tilde{\lambda}_m^*(\omega') \tilde{\lambda}_k(\omega')$ are the overlap of the spectral functions $\tilde{\lambda}_m(\omega')$, which are Fourier transforms of the profile functions $\lambda_m(\tau)$ introduced in Eq. (4.2).

The profile functions $\lambda_m(\tau)$ should be eigenstates for each corresponding azimuthal mode m , when the bunch intensity is small and no mixing occurs. Here, we choose them as the sinusoidal densities introduced by Sacherer. [7]

$$\lambda_m(\tau) = \begin{cases} \frac{\pi}{2\tau_L} \cos \frac{(m+1)\pi\tau}{\tau_L} & m \text{ even} \\ \frac{\pi}{2\tau_L} \sin \frac{(m+1)\pi\tau}{\tau_L} & m \text{ odd} \end{cases} \quad (4.5)$$

The spectral functions are therefore

$$\tilde{\lambda}_m(x) = \begin{cases} i^m \frac{m+1}{2\pi} \frac{\cos \pi x/2}{x^2 - (m+1)^2} & m \text{ even} \\ i^m \frac{m+1}{2\pi} \frac{\sin \pi x/2}{x^2 - (m+1)^2} & m \text{ odd} \end{cases} \quad (4.6)$$

where a dimensionless frequency parameter $x = \omega\tau_L/\pi$ has been introduced, so that, with the exception of $m = 0$, the spectrum for the m th mode peaks at $x \approx m + 1$ and has a full width of $\Delta x \approx 2$, as illustrated in Fig. 2. The revolution angular frequency is therefore given by $x_0 = \omega_0\tau_L/\pi$. We also introduce a dimensionless current parameter

$$\epsilon = -\frac{I_b R_s / n_r}{3B_0^3 h V_0 \cos \varphi_s} , \quad (4.7)$$

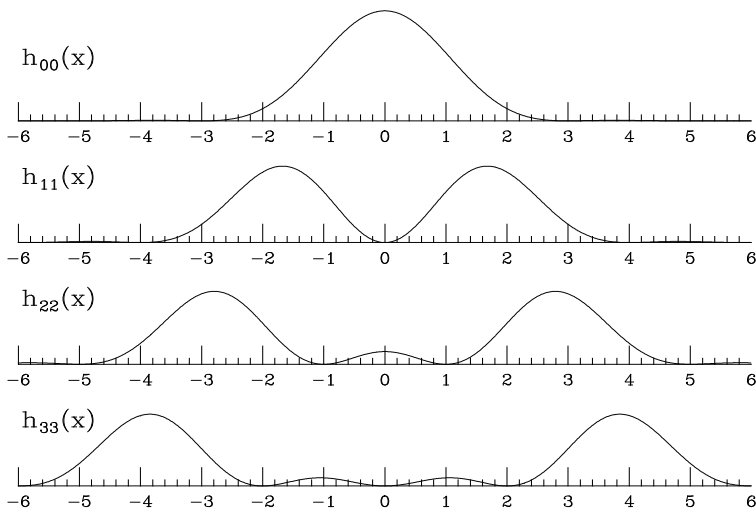


Fig. 2. Some of the power spectra $h_{mm}(x)$ of the sinusoidal modes introduced by Sacherer.

which is positive above transition. Unlike the first factor on the right-hand side of Eq. (4.4), ϵ is proportional to $I_b R_s$ linearly, where R_s is the shunt impedance of the driving resonant impedance centered at $n_r f_0$ or at $x_r = 2n_r f_0 \tau_L$.

For a broad-band impedance the argument $\omega' = n\omega_0 + \Omega$ in the coupling matrix M_{mk} can be replaced by $\omega = n\omega_0$. Then $Z(\omega)$ and $\tilde{\lambda}_m(\omega)$ possess definite symmetries. It is easy to see that all matrix elements are real. We can also see that modes m and k are coupled through $\text{Re } Z$ when $m - k$ is odd, and through $\text{Im } Z$ when $m - k$ is even. For each individual mode m , the shift in coherent frequency is due to the diagonal element M_{mm} driven by $\text{Im } Z$. Above transition ($\eta > 0$ or $\cos \varphi_s < 0$), the inductive impedance shifts the frequency upward, while the capacitive impedance shifts the frequency downward. These shifts can cause two modes to cross each other, but produce no instability because the shifts are real. Instability is contributed by the non-diagonal elements. For two adjacent modes to merge into one and produce instability, the driving force is the real part of the impedance.

Let us continue with the example of the Fermilab Main Ring which has a broad-band impedance centered at $x_r = 7.5$ or $f_r \sim 1.88$ GHz and quality factor $Q \approx 1$. The eigen frequencies obtained from solving Eq. (4.3) are plotted in Fig. 3 versus the current parameter ϵ . We find mode 6 peaks at the inductive part of the resonant impedance and is therefore shifted upward. Mode 7 peaks at the capacitive part of the impedance and is shifted downward. The real part of the resonant peak merges the two modes into one at $\epsilon = 0.94$, after which the bunch becomes unstable. Note that the ordinate of Fig. 3 is normalized with respect to the unperturbed synchrotron frequency ω_{s0} , and an adjustment for the incoherent tune shift

$$\omega_s - \omega_{s0} = \frac{3}{2\pi^2} \frac{\omega_{s0} I_b (Z/n)_{\text{ind}}}{B_0^3 h V_0 \cos \varphi_s} \quad (4.8)$$

has been made. This correction pushes all coherent modes downward. When the current is

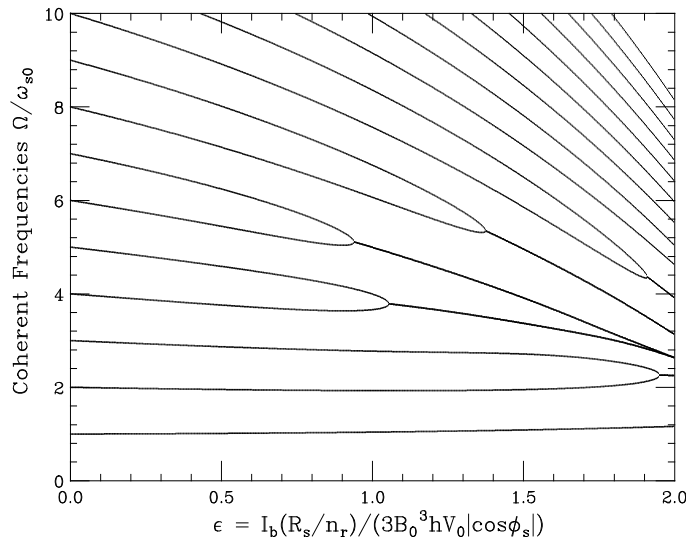


Fig. 3. Coupling of modes $m = 6$ and 7 in the presence of a resonance at $x_r = 7.5$ and $Q = 1$ above transition.

small, the rigid dipole mode $m = 1$ is not shifted at all. This is to be expected because the center of the rigid bunch cannot see any modification of the rf potential due to the bunch itself.

We vary Q and compute the threshold ϵ_{th} in each case. The result is plotted in Fig. 4 versus $z = \Delta f_r \tau_L = x_r/4Q$, where $\Delta f_r = f_r/2Q$ is the HWHM of the resonance. Physically z denotes the ratio of the FWHM of the resonance to roughly the full width of the spectrum of the bunch. Also plotted are threshold curves for resonances centered at different frequencies from $x_r = 3.5$ to 10.5 . Note that all the threshold curves fall roughly on top of each other, and approach a minimum threshold of $\epsilon_{th} \approx 0.92$ when z reaches ~ 0.6 . The latter has the physical meaning of the resonance peak just wide enough to cover only two coupling modes. A smaller z implies that the resonance peak is too narrow and interacts with only parts of the two mode spectra, thus giving a higher instability threshold. A larger z means that the resonance will cover more than two mode spectra. For $x_r = 7.5$ say, modes 6 and 7 will then be pulled and pushed also by the other modes as well so that some cancellation will occur, and one may expect the threshold for their collision to be higher also. However, Eq. (4.4) reveals that the coupling comes in not through $\mathcal{R}e Z(\omega)$ but through $\mathcal{R}e Z(\omega)/\omega$, whose peak value becomes larger and the peak frequency smaller when the quality factor Q is small, although the zero of $\mathcal{I}m Z(\omega)/\omega$ remains unchanged. Figure 5 shows such a plot with $x_r = 7.5$ and $Q = 0.2$, where the peak of $\mathcal{R}e Z(\omega)/\omega$ increases from ~ 1 to 2.6 and the position of the peak shifts to $x = 1.6$. Figure 6 shows the enhancement of $\mathcal{R}e Z(\omega)/\omega$ and its frequency position as the quality factor decreases from 100 to 0.001 . For this reason, when Q is small enough, the lower modes start to collide first. For the case of the resonant broad-band centered at $x_r = 7.5$ and $Q = 0.2$ (or $z = 9.4$), Fig. 7 shows that modes 1 and

2 start to merge first. Thus, the threshold for large z remains small, which is very much different from what Sacherer stated in his paper.

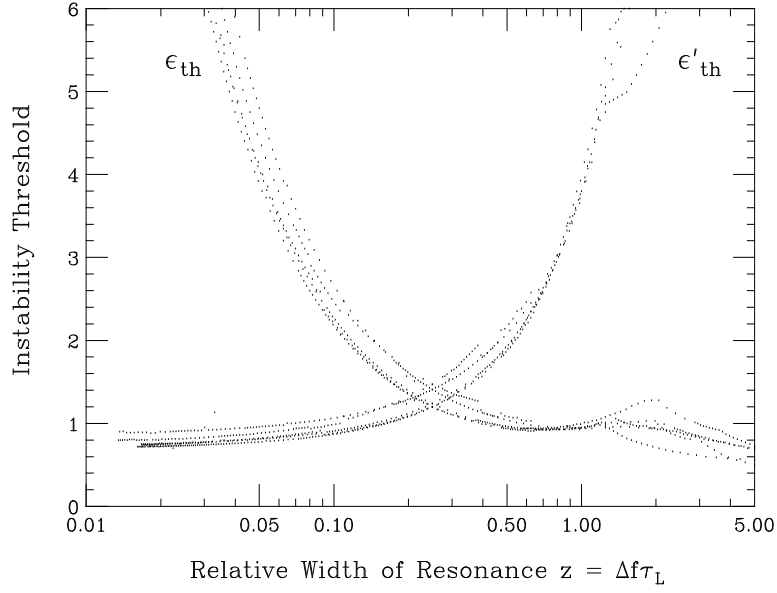


Fig. 4. Instability thresholds ϵ_{th} and ϵ'_{th} for various widths of the resonance impedance located at $x_r = 3.5$ to 11.5 .

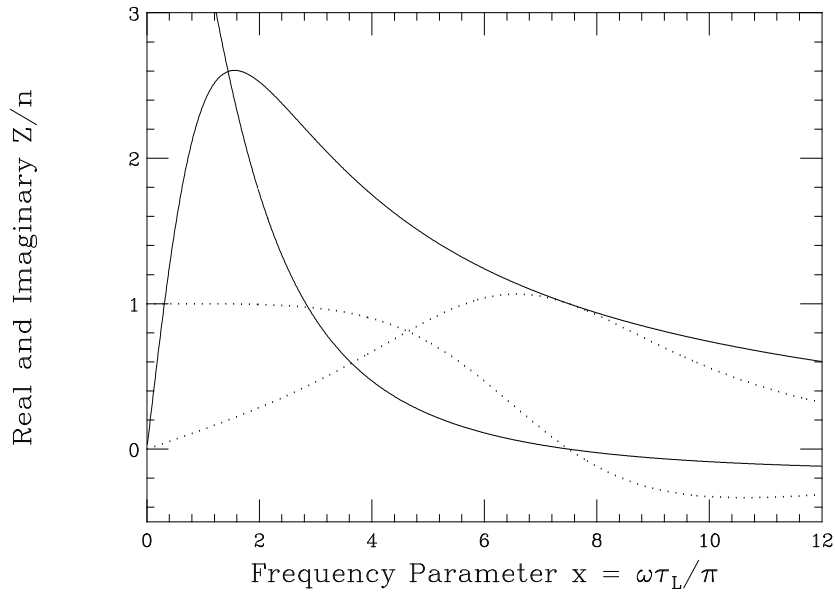


Fig. 5. Comparison of $\mathcal{R}e Z/n$ and $\mathcal{I}m Z/n$ centered at $x_r = 7.5$ for $Q = 1$ (dots) and $Q = 0.2$ (solid). Note that when the resonance becomes broader, the contributions of Z/n move towards lower frequencies.

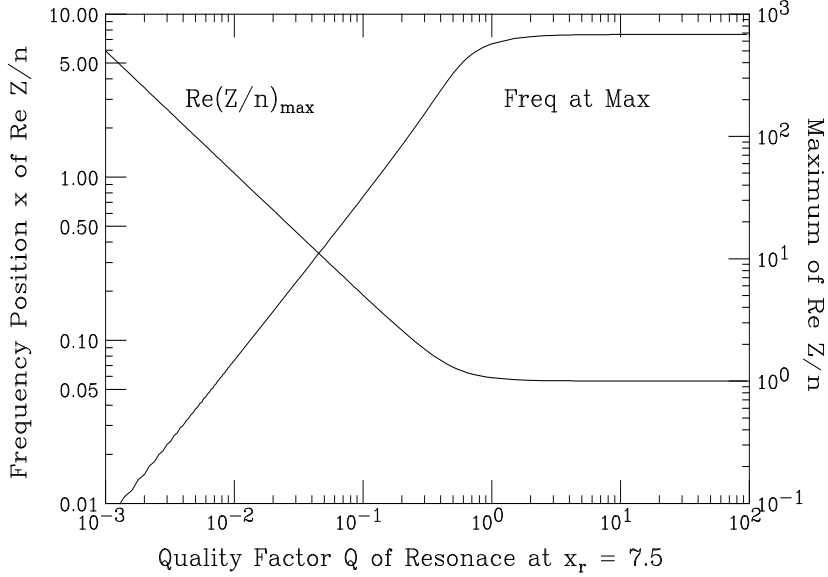


Fig. 6. Enhancement of $(\text{Re}Z/n)_{\text{max}}$ (normalized to R_s) and its frequency position x as the quality factor Q of the resonance centered at $x_r = 7.5$ decreases.

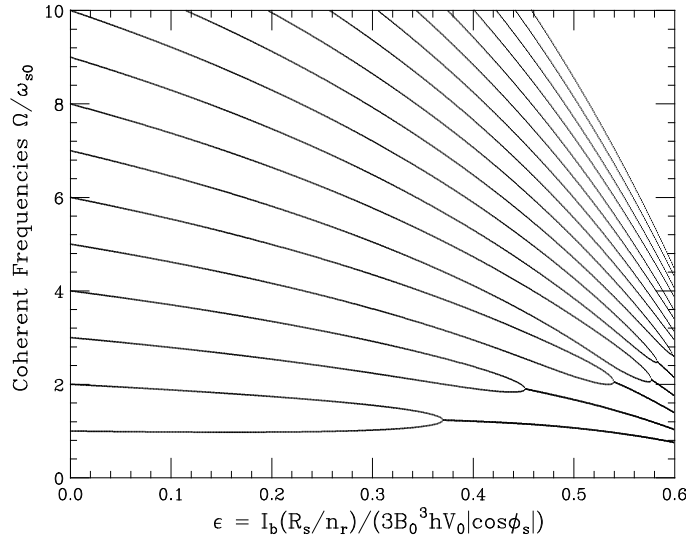


Fig. 7. Mode coupling starts at the lowest modes when the driving resonance is much wider than the bunch spectrum. Here $x_r = 7.5$, $Q = 0.2$, $\tau_L = 2$ ns, or $z = 9.4$.

V. MICROWAVE INSTABILITY DRIVEN BY BROAD RESONANCES

Microwave instability can occur when the resonance is much wider than the bunch spectrum. When this happens, many coherent modes are excited. We see that modes 6 and 7 merge first in Fig. 3 when $Q = 1$ but modes 1 and 2 merge first in Fig. 7 when $Q = 0.2$. In between, when $Q \sim 0.45$, we find that modes 2 and 3, 4 and 5, 6 and 7 start to merge at nearly the same threshold of $\epsilon_{th} \approx 0.75$. Therefore, we can conclude that the threshold

at the $z \gg 1$ end is the threshold of microwave instability. This threshold condition can be easily rewritten in terms of the energy spread $(\Delta E)_{\text{FWHM}} = \frac{3}{2}(\Delta E)_{\text{full}}$ and bunch peak current $I_p = \pi I_b / (2\tau_L f_0)$ of the sinusoidal profile as

$$\frac{R_s}{n_r} = \frac{27}{16} \epsilon_{th} \frac{\eta(E/\epsilon)}{I_p} \left(\frac{\Delta E}{E} \right)_{\text{FWHM}}^2, \quad (5.1)$$

which is the familiar Boussard-modified Keil-Schnell criterion [1] of microwave instability driven by a broad resonance. The form factor for this type of cosine bunch shape should be close to unity, which is close to $\frac{27}{16} \epsilon_{th} = 1.3$ obtained here. The equivalence of mode-coupling and microwave instability had been pointed out by Sacherer [6] and Laclare. [8]

The threshold ϵ_{th} can also be estimated. When the resonant impedance $\mathcal{R}e Z$ is just wide enough to cover two adjacent modes m and $m' = m + 1$, and the excitation is one with $x_r = \frac{1}{2}(m + 3)$ nodes along the bunch, the coupling matrix can be truncated to include only these two modes. The coupling matrix of Eq. (4.5) can be rewritten as

$$M_{mm'} = \epsilon A_{mm'}, \quad (5.2)$$

or

$$A_{mm'} = \frac{i \sum_n h_{mk}(n) [n_r \hat{Z}(n)/n]}{\sum_n h_{mm}(n)}, \quad (5.3)$$

where $\hat{Z}(n) = Z(n)/R_s$. In above, the factor $\frac{m}{m+1}$ as well as the difference between ω_s and ω_{s0} have been neglected. The eigen equation (4.3) now becomes

$$\begin{vmatrix} \frac{\Omega}{\omega_{s0}} - m - \epsilon A_{mm} & \epsilon A_{mm'} \\ \epsilon A_{m'm} & \frac{\Omega}{\omega_{s0}} - m' - \epsilon A_{m'm'} \end{vmatrix} = 0, \quad (5.4)$$

from which we obtain, with $A_{mm'} A_{m'm} = -|A_{m'm}|^2$,

$$\Omega = \frac{1}{2} \omega_{s0} \left[(\nu_m + \nu_{m'}) \pm \sqrt{(\nu_{m'} - \nu_m)^2 - 4\epsilon^2 |A_{mm'}|^2} \right], \quad (5.5)$$

where $\nu_k = k + \epsilon A_{kk}$, $k = m$ or m' . The threshold of instability ϵ_{th} is therefore given by

$$|\epsilon_{th} A_{mm'}| = \frac{1}{2} |\epsilon_{th} (A_{m'm'} - A_{mm}) + 1|. \quad (5.6)$$

The matrix elements A_{mm} , $A_{m'm'}$, and $A_{mm'}$ have been computed numerically for any two adjacent m , m' , with the resonance peak centered at $x_r = \frac{1}{2}(m + 3)$. The result is actually very close to $\epsilon_{th} = 0.92$ and depends on m very weakly. It can also be estimated easily. We first neglect A_{mm} and $A_{m'm'}$, and get $|\epsilon_{th} A_{mm'}| \approx \frac{1}{2}$. We can approximate the resonance $\mathcal{R}e Z(x)/x$ by a rectangular box of height R_s/x_r and width wide enough to contain the two coupling adjacent spectra, as illustrated in Fig. 8. Each spectral function $\tilde{\lambda}_m(x)$ can also be approximated by a rectangular box of total width $\Delta x = 2$. Since the two spectra are adjacent, the overlap is $\Delta x = 1$. Therefore, we obtain $|\sum_n \tilde{\lambda}_m^*(n) \tilde{\lambda}_{m'}(n)| \approx \frac{1}{2} \sum_n \tilde{\lambda}_m^*(n) \tilde{\lambda}_m(n)$ or $|A_{mm'}| \approx \frac{1}{2}$; thus $\epsilon_{th} \approx 1$. We can now include A_{mm} and $A_{m'm'}$ by further approximating $\mathcal{I}m Z(x)/x$ by R_s/x_r when $x < x_r$ and $-R_s/x_r$ when $x > x_r$. We obtain $A_{mm} \approx -A_{m'm'} \approx \frac{1}{2}$, which is an overestimate, and $\epsilon_{th} = \frac{1}{2}$. Therefore, $\frac{1}{2} < \epsilon_{th} < 1$.

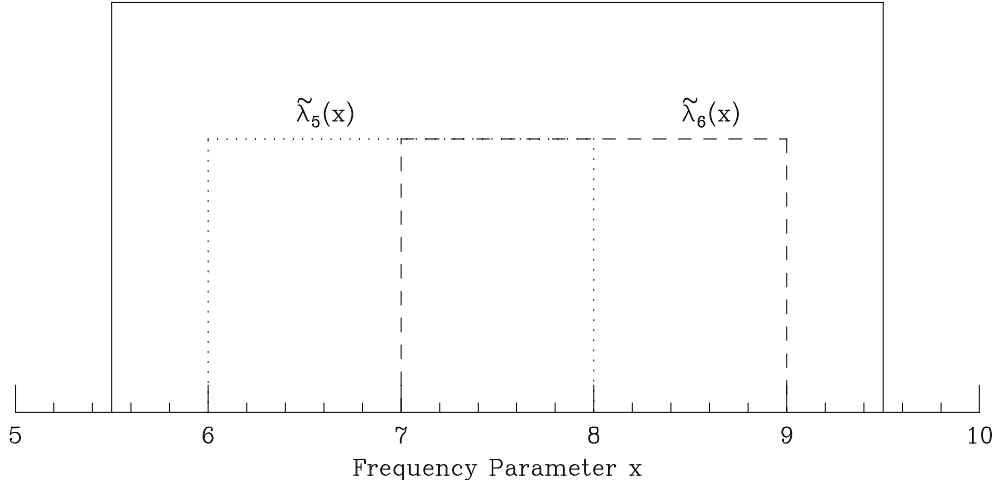


Fig. 8. An estimate of the nondiagonal coupling matrix elements by rectangularizing $\text{Re } Z$ and the adjacent coupling spectral modes.

VI. MICROWAVE INSTABILITY DRIVEN BY NARROW RESONANCES

When the resonance is much narrower than the width of the bunch spectrum, we have $z \ll 1$. Then, the summation over frequency in Eq. (3.2) can be approximated by

$$\sum_n \frac{x_r Z(n)}{n} h_{mm'}(n) \approx \frac{\pi R_s x_r}{Q} \tilde{\lambda}_m^* \tilde{\lambda}_{m'} |_{x=x_r} . \quad (6.1)$$

Since the area under the narrow resonance is concerned here, a new dimensionless current parameter

$$\epsilon' = -\frac{2I_b(R_s/Q)}{3B_0^2 h V \cos \phi_s} \quad (6.2)$$

is required. This new threshold ϵ'_{th} is now plotted versus z in Fig. 4. For small z , we obtain $\epsilon'_{th} \approx 0.75$ which is almost independent of x_r . Again, this threshold can be computed numerically using the truncated 2×2 coupling matrix, or estimated by approximating the spectral functions by rectangular curves. When it is cast into the form

$$\frac{R_s}{Q} = \frac{27}{16\pi} \epsilon'_{th} \frac{\eta(E/e)}{I_b} \left(\frac{\Delta E}{E} \right)_{\text{FWHM}}^2 , \quad (6.3)$$

it is just the criterion of microwave instability driven by an impedance resonance that is narrower than the bunch spectrum. [2] The form factor is 0.41, which agrees very well with $\frac{27}{16\pi} \epsilon'_{th} \approx 0.40$. This may be a more appropriate microwave instability threshold for electron machines, since electron bunches are short.

We have computed the mode-mixing for our former Main Ring bunch when the driving resonant impedance is narrow with a $Q = 100$. The result in Fig. 9 gives a threshold of

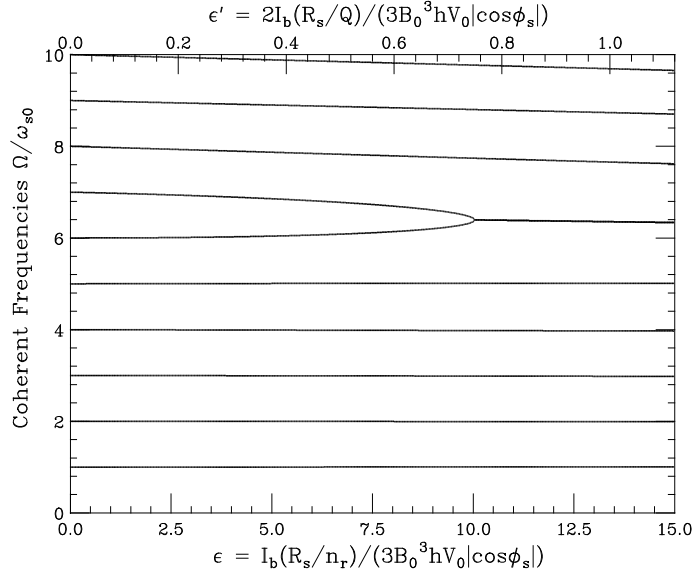


Fig. 9. Coupling of modes $m = 6$ and 7 in the presence of a narrow resonance at $x_r = 7.5$ and $Q = 100$ above transition.

$\epsilon_{th} = 10.0$ (or $\epsilon'_{th} = 0.75$), which is much larger than that for the broad-band impedance. This increase in threshold has been explained in Sec. IV, and is a result of the fact that the narrow resonance interacts with only a small part of the overlapping spectra. We also see that, as ϵ increases, the coherent frequencies here do not shift so much lower than the situations in Figs. 3 and 7. This is because the resonances there are rather broad and their contributions move towards lower frequencies (Fig. 5).

VII. GOING BELOW TRANSITION

Figure 3 shows that the coherent frequencies tend to cluster together when the current ϵ increases. This is because we are above transition, $\cos \varphi_s < 0$. Looking into the diagonal elements of Eq. (4.4), modes with $m < x_r - 1$ ($> x_r - 1$) sample the inductive (capacitive) part of the impedance and are shifted upward (downward). Below transition, the shifts will be in the opposite direction; i.e., diverging outward with increasing $|\epsilon|$. Mathematically, $(\nu_{m'} - \nu_m)^2$ inside the square root of Eq. (5.5) becomes larger. However, this does not mean that there will be no instability. This is because the off-diagonal elements $\epsilon A_{mm'}$ that are responsible for mode merging contribute as squares and therefore do not change sign. In fact, from Eq. (5.5), we obtain the threshold

$$|\epsilon_{th}| = \frac{1}{2|A_{mm'}| - |A_{m'm'} - A_{mm}|} \quad (7.1)$$

below transition, and

$$\epsilon_{th} = \frac{1}{2|A_{mm'}| + |A_{m'm'} - A_{mm}|} \quad (7.2)$$

above transition. It is now clear why the threshold below transition is much higher than the threshold above transition. We tried to reverse the sign of $\cos \varphi_s$ in the example of Fig. 3 to obtain Fig. 10 and found $|\epsilon_{th}|$ actually increases from 0.94 to 1.88. This is also true for narrow resonances; Fig. 9 becomes Fig. 11 below transition with $|\epsilon'_{th}|$ increases from 0.75 to 1.8. This conclusion is in sharp contradiction to the statement of Laclare [8] that “below transition mode coupling cannot lead to instability.”

The above discussion leads to the conjecture that a bunch in a machine with a negative momentum-compaction factor [9] will be more stable. This idea had been pointed out by Fang et al [10] in obtaining shorter electron bunches for colliders.

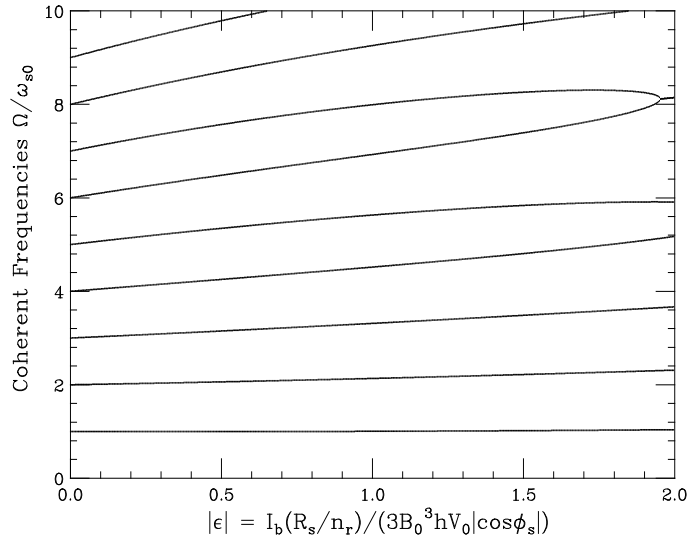


Fig. 10. The situation of Fig. 3 below transition. Note the increase in threshold $|\epsilon_{th}|$.

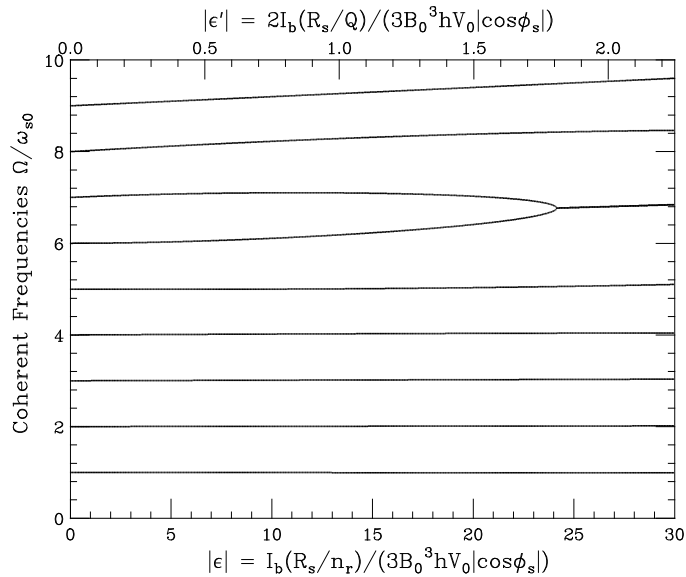


Fig. 11. The situation of Fig. 9 below transition. Note the increase in threshold $|\epsilon'_{th}|$.

VIII. CONCLUSIONS

We have explored the effects of potential-well distortion and mode mixing for proton bunches. Applications have been made to the Main Ring bunches and the future Main Injector bunches. Due to the long length of a proton bunch, the spectrum of its profile sees mostly only the inductive part of the broad-band coupling impedance. As a result, potential-well distortion only amounts to the lengthening of the bunch with very little head-tail asymmetry. A Main Ring bunch will be lengthened by $\sim 5\%$. The higher-order modes, however, can see the peak of the real part of the impedance, which will drive adjacent modes to merge together to produce instability. When the resonant impedance is much wider than the spectrum of the bunch, this mode-mixing threshold is equivalent to the threshold of the Boussard-modified Keil-Schnell criterion of microwave instability. When the resonant impedance is much narrower than the spectrum of the bunch, such as in electron machines, the mode-mixing threshold is equivalent to the threshold of microwave instability driven by narrow resonances. For short electron bunches, usually it is modes 1 and 2 that collide first as the bunch intensity increases. For proton bunches, however, higher modes start to collide first unless the impedance is extremely broad. This is because the proton bunch usually has a length equal to many cut-off wavelengths of the vacuum chamber. We have also discussed the situation when the machine operates below transition and found that the threshold will be pushed to a larger value and thus becoming more stable.

The complete equivalence of mode-coupling instability and microwave instability has not been established here. For example, we have not addressed the microwave instability driven by a pure space-charge impedance above transition. If we carry out an analysis similar to that in Sec. V, we find that coupling occurs only between modes m and m' with $|m - m'| = 2, 4, \dots$. Then, a coupling element and its conjugate gives $A_{mm'}A_{m'm} = |A_{m'm}|^2$ instead, or the discriminant in Eq. (5.5) will be positive definite. In other words, there will not be any instability, contrary to the negative-mass instability observed just after transition. This and other issues will be examined further and reported elsewhere.

APPENDIX

In this Appendix, we derive the equation for coupled bunch modes of (4.3). The Vlasov Equation with canonical variables

$$\begin{cases} q = \tau \\ p = -\frac{\eta}{\omega_s}\delta \end{cases}, \quad (\text{A.1})$$

is given by

$$\frac{\partial\psi}{\partial s} + \frac{\partial\psi}{\partial q}q' + \frac{\partial\psi}{\partial p}p' = 0, \quad (\text{A.2})$$

where the ‘prime’ denotes derivative with respect to s , the distance along the ring. The distribution function ψ is written as unperturbed part ψ_0 plus a perturbed part ψ_1 having a coherent frequency Ω :

$$\psi(r, \phi) = \psi_0(r) + \psi_1(r, \phi)e^{-i\Omega s/c}, \quad (\text{A.3})$$

where the polar coordinates defined in Eq. (4.1) has been used. When the effect of the wake potential is included, the Hamiltonian equations are

$$q' = -\frac{\nu_s}{R}r \sin \phi, \quad (\text{A.4})$$

and

$$p' = -\frac{\nu_s}{R}r \cos \phi + \frac{e^2\eta}{2\pi RE\nu_s} \sum_n \tilde{\rho}_1(\omega') Z(\omega') e^{i\omega'\tau - i\Omega s/c}, \quad (\text{A.5})$$

where $\omega' = n\omega_0 + \Omega$ and the spectrum of the perturbed linear distribution is defined as

$$\tilde{\rho}_1(\omega) = \frac{1}{2\pi} \int d\tau d\delta e^{-i\omega\tau} \psi_1(\tau, \delta). \quad (\text{A.6})$$

The perturbed distribution is now expanded into azimuthal harmonics in the longitudinal phase space

$$\psi_1(r, \phi) = \sum_m \alpha_m R_m(r) e^{im\phi}. \quad (\text{A.7})$$

Multiplying by $e^{-im\phi}$ and integrating over ϕ , the Vlasov equation becomes

$$(\Omega - m\omega_s)\alpha_m R_m(r) = \frac{i^{m-1}m e^2\eta}{2\pi RE\nu_s} \frac{\psi'_0}{r} \sum_n \tilde{\rho}_1(\omega') J_m(\omega'r) \frac{Z(\omega')}{\omega'}, \quad (\text{A.8})$$

where $\psi'_0 = d\psi_0/dr$. Changing the variables from (τ, δ) to (r, ϕ) and substituting Eq. (A.7), the perturbed spectrum of Eq. (A.6) can be simplified to

$$\tilde{\rho}_1(\omega) = \sum_m \alpha_m \tilde{\lambda}_m(\omega), \quad (\text{A.9})$$

where

$$\tilde{\lambda}_m(\omega) = \frac{i^{-m}\omega_s}{\eta} \int_0^\infty dr r R_m(r) J_m(\omega r) \quad (\text{A.10})$$

is the Fourier transform of the perturbed bunch linear density corresponding to azimuthal harmonic m . At low bunch intensity, for each m , the various radial modes can be denoted by $R_{mq}(r)$ with $q = 1, 2, \dots$. Since we are going to neglect radial modes, we only include the “most coherent” one with $q = m$. Then, $\tilde{\lambda}_m(\omega)$ peaks at $\omega \approx (m+1)\pi/\tau_L$, and the corresponding perturbed linear density $\lambda_m(\tau)$ has m nodes. Relation (A.10) can also be inverted to read

$$R_m(r) = \frac{i^m \eta}{\omega_s} \int_0^\infty d\omega \omega \tilde{\lambda}_m(\omega) J_m(\omega r) . \quad (\text{A.11})$$

Using Eq. (A.10), the Vlasov equation can be transformed from Eq. (A.8) to

$$(\Omega - m\omega_s)\alpha_m \int_0^\infty dr |R_m(r)|^2 \frac{r^2}{\psi'_0} = -\frac{im\epsilon^2\eta^2}{2\pi\nu_s^2 E} \sum_n \tilde{\rho}_1(\omega') \frac{Z(\omega')}{\omega'} \tilde{\lambda}_m^*(\omega') . \quad (\text{A.12})$$

Substituting the harmonic expansion of $\tilde{\rho}_1$, we arrive at the eigen-equation

$$(\Omega - m\omega_s)\alpha_m = \sum_k \left[\frac{im\epsilon^2\eta^2 \sum_n \tilde{\lambda}_k(\omega') \frac{Z(\omega')}{\omega'} \tilde{\lambda}_m^*(\omega')}{2\pi\nu_s^2 E \int_0^\infty dr |R_m(r)|^2 \frac{r^2}{\psi'_0}} \right] \alpha_k , \quad (\text{A.13})$$

which is of the same form as Eq. (4.3).

Finally, we need to compute the integral in the denominator of Eq. (A.13). We can write

$$\int_0^\infty dr |R_m(r)|^2 \frac{r^2}{\psi'_0} = \left\langle \frac{r}{\psi'_0} \right\rangle \int_0^\infty dr r |R_m(r)|^2 , \quad (\text{A.14})$$

where $\langle r/\psi'_0 \rangle$ denotes some characteristic value of r/ψ'_0 . Since ψ_0 is normalized to $\eta N/\omega_s$ and depends on τ_L only, we must have

$$\left\langle \frac{r}{\psi'_0} \right\rangle \propto -\frac{\omega_s \tau_L^4}{\eta N} . \quad (\text{A.15})$$

The integral on the right side of Eq. (A.14) can now be performed with the aid of Eq. (A.11) to give

$$\int_0^\infty dr r |R_m(r)|^2 = \frac{\eta^2}{\omega_s^2} \int_0^\infty d\omega \omega |\tilde{\lambda}_m(\omega)|^2 . \quad (\text{A.16})$$

We next make use of the fact the $\tilde{\lambda}_m(\omega)$ has definite symmetry and peaks at $\omega \sim (m+1)\pi/\tau_L$. Then,

$$\int_0^\infty d\omega \omega |\tilde{\lambda}_m(\omega)|^2 \approx \frac{(m+1)\pi\omega_0}{2\tau_L} \sum_{n=-\infty}^\infty |\tilde{\lambda}_m(\omega')|^2 , \quad (\text{A.17})$$

Combining Eqs. (A.14) to (A.17), eigen-equation (A.13) takes the form

$$(\Omega - m\omega_s)\alpha_m = -F \sum_k \left[\frac{im I_b \omega_s \omega_0}{3(m+1)B_0^3 h V_T \cos \varphi_s} \frac{\sum_n \tilde{\lambda}_k(\omega') \frac{Z(\omega')}{\omega'} \tilde{\lambda}_m^*(\omega')}{\sum_n |\tilde{\lambda}_k(\omega')|^2} \right] \alpha_k , \quad (\text{A.18})$$

where F is a form factor which is of $\mathcal{O}(1)$, depending on the form of the unperturbed distribution $\psi_0(r)$. For example, if we choose

$$\psi_0(r) = \frac{32\eta N}{\pi\omega_s\tau_L^4} \left(\frac{\tau_L^2}{4} - r^2 \right), \quad (\text{A.19})$$

so that

$$\frac{\psi'_0}{r} = -\frac{64\eta N}{\pi\omega_s\tau_L^4} \quad (\text{A.20})$$

is no longer r -dependent, we obtain $F = 96/\pi^4 = 0.986$.

References

- [1] D. Boussard, CERN/LAB II/RF/75-2 (1975); E. Keil and W. Schnell, CERN/ISR/TH/RF/69-48 (1969)
- [2] K.Y. Ng, Proc. 1986 Summer Study on Phys. of SSC, ed. R. Donalson and J. Marx, 1986, p.590.
- [3] K.Y. Ng, Proc. 1995 Particle Accelerator Conference, Dallas, Texas, May 1-5, 1995.
- [4] J. Haïssinski, Nuovo Cimento **B18**, 72 (1973).
- [5] A.W. Chao, *Physics of Collective Beam Instabilities in High Energy Accelerators*, Wiley, p.284.
- [6] F.J. Sacherer, IEEE Trans. Nucl. Sc. **24**, No.3, 1393 (1977).
- [7] F.J. Sacherer, CERN Internal Report CERN/SI-BR/72-5.
- [8] J.L. Laclare, CERN Accel. School, Queen's College, Oxford, England, 1985, p.264.
- [9] S.Y. Lee, K.Y. Ng, and D. Trbojevic, Phys. Rev. **E48**, 3040 (1993).
- [10] S.X. Fang, K. Oide, Y. Yokoya, B. Chen, and J.Q. Wang, KEK Preprint 94-190, 1995.